

Improving Attribution Methods by Learning Submodular Functions

Piyushi Manupriya, Saketha Nath Jagarlapudi, Tarun Ram Menta, and
Vineeth N Balasubramanian

Indian Institute of Technology, Hyderabad

Abstract. This work explores the novel idea of learning a submodular scoring function to improve the specificity/selectivity of existing feature attribution methods. Submodular scores are natural for attribution as they are known to accurately model the principle of diminishing returns. A new formulation for learning a deep submodular set function that is consistent with the real-valued attribution maps obtained by existing attribution methods is proposed. This formulation not only ensures that the scores for the heat maps that include the highly attributed features across the existing methods are high, but also that the score saturates even for the most specific heat map. The final attribution value of a feature is then defined as the marginal gain in the induced submodular score of the feature in the context of other highly attributed features, thus decreasing the attribution of redundant yet discriminatory features. Experiments on multiple datasets illustrate that the proposed attribution method achieves higher specificity while not degrading the discriminative power.

Keywords: Neural Network Interpretability · Attribution Algorithm · Submodularity

1 Introduction

Deep neural networks (DNNs) have shown state-of-the-art performance in diverse application domains, including complex tasks such as image recognition, video synthesis, speech-to-text conversion and autonomous navigation, to name a few. While advancements in deep learning have led to increasing accuracy scores, this has often been at the expense of the interpretability of the neural network’s decisions. Interpretability of DNNs is important not only to foster trust in their predictions, but also to debug these complex networks. Over the last few years, there have been a diverse set of approaches for interpretability, some of which include visualizing weights of a trained model [30], approximating the original model with an interpretable surrogate model [19], performing case-based reasoning [5], modifying the training procedure [31] and quantifying feature importances using attribution algorithms [3, 15, 23, 28, 30]. Our work focuses on attribution algorithms for neural networks trained for image classification. These algorithms output an attribution score map that represents the

feature-wise contribution of each input feature towards the prediction, a topic that has attracted significant interest in recent years.

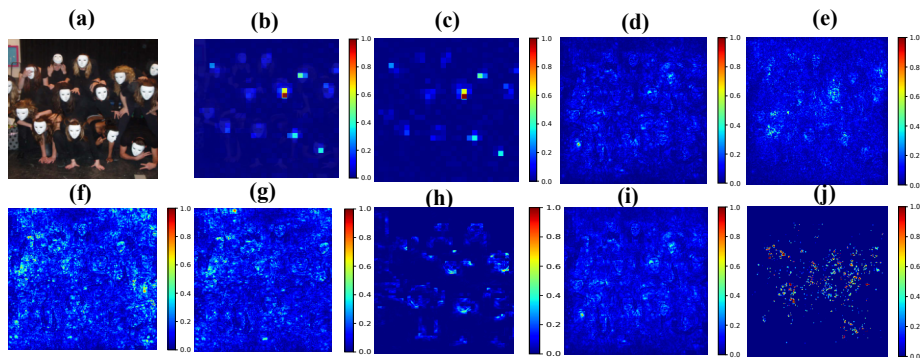


Fig. 1. (a) Image belonging to class Mask (b) SEA-NN(proposed) map overlaid on image (c) SEA-NN (d) IG (e) SIG (f) DL (g) DL-SHAP (h) GGC (i) Agg-Mean (j) CASO

As shown in Fig 1, attribution algorithms provide a normalized score for each input feature (pixels in case of image-based problems, where such methods are extensively used), which denotes its contribution to the prediction on the given input. Existing attribution algorithms assign this score based on different strategies such as occluding the pixel under consideration [30], backpropagating across the model to the input [27], computing the gradient of the output w.r.t a particular input [4, 22, 32], or considering additional inputs as baselines to compute gradients [23, 28].

Our approach in this work is based on the observation that attribution heat maps obtained by existing methods (e.g. refer Fig 1) are not sharply focused around the discriminatory pixels and are often liberally spread out across the image. In other words, though existing algorithms achieve good sensitivity, they do not seem to achieve high specificity/selectivity. The key idea here is to employ a monotone submodular set function for scoring the heat maps, such that the scores for the most specific of the given maps are themselves saturated.

However, such a submodular function is neither known nor designed in existing literature. We hence propose a novel algorithm that *learns* one based on the heat maps with existing attribution algorithms. Learning such a submodular function across multiple attribution algorithms provides us a mechanism to summarize these methods, as well as provides attribution maps that are consistent across methods. The works closest to ours include [20], which performs pixel-wise averaging of attribution maps, and [7], which uses cardinality-constrained submodular optimization to select top- k important pixels. We compare against [20]

in this work, and show that our ensembled attribution map guided by a learnt submodular scoring function outperforms simple linear averaging. [2] also aggregates attribution maps to enhance their sparsity, however, their algorithm is focused on tabular data. [7] uses the notion of weak submodularity for interpretability in a streaming setting (different from ours), and was intended for selection of a subset of features, rather than assigning attribution scores. Also, as noted by them, the function that they use is neither expected to be monotone nor submodular.

Once the submodular scoring function is induced, we present our new model-agnostic attribution algorithm **Submodular Ensembled Attribution for Neural Networks(SEA-NN)**, that scores features according to their marginal score gains in presence of other critical features, rather than attributing according to the raw scores. This encourages specificity as the redundant yet discriminatory features get less attributed. We note that the computational overhead of learning the submodular score and the computation attribution is not prohibitive and is limited to some neural network evaluation and backpropagation calls, which can be very efficiently implemented.

Since there are no well-established benchmarks for studying goodness of attribution scores, each such method has different biases in defining what may or may not be important in an input. To address this issue, our proposed methodology assigns attribution scores to input features that are consistently responsible across multiple attribution algorithms for a given input-output pair on a given model. One could also view such a methodology as summarizing multiple attribution algorithms for a given DNN model. Additionally, as shown by [21], the adversarial attacks on attribution algorithms don't transfer well between different attribution methods making methods that aggregate attribution maps of different methods more robust to such attacks. As DNN models penetrate critical application domains such as healthcare, criminal justice and finance, such an approach becomes timely and necessary.

Our experimental results across multiple datasets show that our results consistently show brevity and outperform existing attribution methods on the considered metrics. Moreover, if each of our input attribution methods satisfy the axioms of attribution defined in [28], we argue that our method either inherits them or can be easily modified to satisfy them.

The key contributions of our work can be summarized as follows: (i) We propose a new formulation for learning a submodular set function from real-valued heat maps. Typical supervision studied in literature for learning submodular functions is of the form of a collection of "important" subsets rather than real-valued importance maps. We hence believe the proposed formulation may be of independent interest in other applications of submodular learning; (ii) We propose the algorithm, Submodular Ensembled Attribution for Neural Networks(SEA-NN), which improves over existing attribution methods in several ways; (iii) We show how SEA-NN has some unique advantages, including being employed for attributing features across a set of examples (say, ones belonging to a particular class), thus providing both local and global explanations;

(iv) We conduct experiments on well-known image datasets including ImageNet, Brain Tumor Detection, CUB, MNIST and validate the usefulness of the proposed method from a qualitative as well as quantitative perspective; and (v) We propose a simple yet novel Minimal Discriminative Region Size (MDRS) metric to simultaneously measure the discriminative power and sparsity/specificity of an attribution method.

2 Related Work

Attribution algorithms have become one of the most popular research areas in interpretable machine learning in recent years. Prior work in this area can be broadly grouped into occlusion-based, backpropagation-based, perturbation-based approaches. Initial efforts to quantify the importance of patches involved occluding them and doing forward passes to observe the change in output [30]. Due to multiple forward passes, the time taken by occlusion-based methods is a major drawback. Deconvnet was introduced as a backpropagation-based approach in [30]. GuidedBackprop [27] later modified Deconvnet to obtain a cleaner visualization. Layer-wise Relevance Propagation [15] distributed the output score to all the neurons present in a layer and backpropagated in this manner upto the input layer. Another line of work proposed in [24], known as input-grad, involved computing hadamard product of input and partial gradients of output of the desired class wrt each input feature. [32] introduced a modified architecture of CNNs to come up with CAM (Class Activation Map). However, their method required re-training the network which motivated Grad-CAM [22] and later a more generalized version Grad-CAM++ [4]. Saturating gradients came up as the main challenge for gradient-based methods which DeepLift [23] and Integrated Gradients [28] tried to alleviate. A key element in these algorithms is the chosen baseline, ideally coming from the domain knowledge. [3] tried to overcome the dependency on baselines by presenting an adaptive baseline & also proposed a Causal attribution algorithm. For commonly used DNNs with piecewise linear activation functions, gradients represent weights of the network. Gradients are still the most popular ingredient of attribution algorithms and can be looked as a perturbation-based approach.

Unlike most existing attribution algorithms, which assign attribution scores independently to each features, SEA-NN assigns attribution score to a feature in the context of other features. We note that state-of-the-art DNN models are designed to leverage feature inter-dependencies, which should be taken into account while computing attribution scores. As stated earlier, [7] uses the notion of weak submodularity for interpretability in a streaming setting, and was intended for selection of a subset of features, not assignment of attribution scores. [25] propose Context Aware Second-Order Interpretation (CASO), which computes attribution scores of group features, but ignores the inter-dependency between different groups of features. Our choice of modeling using submodular functions makes our attribution maps consider marginal gain of a feature over another

group of features, makes the maps inherently sparse, as well as allows us to ensemble attribution maps, which CASO doesn't.

In terms of metrics for evaluation of attribution methods, popular quantitative evaluation metrics for attribution algorithms include Area Under Perturbation Curve (AUPC) [15], Faithfulness [1], Causal Metric [17] and ROAR [9]. The computation of AUPC involves deletion of pixels (setting them to 0) in the original image in the order of their relevance. After each iteration of removal of pixels, the DNN's softmax score is stored. AUPC is computed as the area under curve of DNN's outputs at different iterations. If the most relevant pixels are removed, a lower AUPC is desired. The other evaluation metrics also largely measure variants of correlation between the attribution score of pixels and the change in DNN's softmax score on removing those pixels. Deletion metric proposed in [17] computes AUPC after deleting pixels in batches. Complexity metric recently proposed in [2] focuses on ranking the attribution methods only according to the sparsity of their attribution maps while our proposed MDRS measures both the specificity and the discriminative power, which we describe in our Methodology section. ROAR removes the most salient pixels from all the images of a dataset and then re-trains the classifier multiple times. The amount of drop in accuracy determines the goodness of the attribution method. Due to multiple retraining involved in computation of ROAR, it makes it computationally prohibitive for us to use it in our experiments. We use AUPC and MDRS in our experiments to study the proposed method.

2.1 Background

Our work builds upon properties of submodular functions. Submodular functions are a special kind of discrete functions, characterized by the diminishing returns property, and appear naturally in many discrete maximization problems like clustering, sensor placement and document summarization [12]. For a set function $f : 2^V \rightarrow \mathbb{R}$ defined on a ground set V , the marginal gain on adding an element e in the context of set A can be defined as $f(e|A) = f(A \cup e) - f(A)$. f is said to be submodular if for any $e \notin B$, for all $A \subseteq V$ and $B \subseteq V$ such that $A \subseteq B$, $f(e|A) \geq f(e|B)$ i.e. the smaller set has a larger gain on addition of a new element. On the other hand, if both sets have equal marginal gain i.e. $f(e|A) = f(e|B)$, then f is said to be modular. In most applications where f acts as a valuation function, f is desired to be non-negative i.e. $f(A) \geq 0$ for all $A \subseteq V$. Additionally, if $f(A) \leq f(B)$ for all $A \subseteq B$, then f is said to be monotonic.

3 Proposed Methodology

Given a neural network with n input features, we assume that we have access to m attribution algorithms that are faithful to it. We denote the heat map (with normalized values in $[0, 1]$) obtained by the i^{th} algorithm on a given input/image as $\mathcal{H}_i \in [0, 1]^n$. We assume that the algorithms are reasonable baselines and

hence, in general, the features that have very high attribution values are indeed critical for discriminatory power of the network.

We focus on devising a new algorithm that improves over the attribution maps that we ensemble. To this end, we first define a scoring function, $f : 2^V \rightarrow \mathbb{R}^+$, where V is the set of pixels, this function assigns a non-negative score to a subset of pixels chosen from the input image consisting of n pixels. Note that f is not a new per-pixel attribution score, but an importance score for a subset of pixels. We also denote f 's real-valued extension by $f_{ext} : [0, 1]^n \mapsto \mathbb{R}^+$. Note that f_{ext} scores attribution heat maps rather than individual features or feature sets. The desirable properties of such a scoring function, given m attribution heat maps as input, are: (1) The score for the baseline heat maps must be high. (2) The score for a heat map with high specificity/selectivity is high; further increasing attribution values in a selective heat map does not increase the score significantly. (3) A discriminatory feature when included in a smaller set of other such features leads to larger improvement of score than when included in a larger set. Note that properties (2) and (3) are critical as attribution based on such scoring functions will promote heat maps with high specificity. Since such scoring functions are not readily available, we propose to learn an appropriate scoring function for this purpose.

3.1 Learning the Scoring Function

While ensuring property (1) above is straight-forward, property (2) and (3) suggest that the proposed scoring function satisfies the so-called diminishing returns property. Accordingly, we model f by monotone submodular functions and f_{ext} by monotone concave functions. This is because submodular functions and their concave extensions are known to accurately model the principle of diminishing returns. And together with monotonicity, such functions allow us to satisfy Property (2) and facilitate early enough saturation of values. Another pragmatic reason for making this choice is that models inducing monotone submodular functions are well-understood [6]. The work [6] proposes a class of functions known as Deep Submodular Functions (DSFs), which can be efficiently learned using appropriate neural network training techniques. We refer the reader to [6] for further details of DSFs and their parametrization.

Let $f_{\mathbf{w}}$ denote a DSF, parameterized by network parameters, $\mathbf{w} > 0$. As argued in [6], $f_{\mathbf{w}}$ restricted to binary valued inputs, $\{0, 1\}^n$, is indeed a monotone submodular function. We make a critical observation here that when such an $f_{\mathbf{w}}$ is relaxed to the domain $[0, 1]^n$, it is indeed a valid concave extension of this submodular function. This is because the activation functions in the network defining the DSF are all non-negative, monotone (increasing), and concave functions. We propose to learn the parameters \mathbf{w} by solving the following novel (intermediate) formulation:

$$\min_{\mathbf{w} \geq 0} \frac{\lambda}{2} \|\mathbf{w}\|^2 + \sum_{i=1}^m [f_{\mathbf{w}}(\mathcal{H}^*) - f_{\mathbf{w}}(\mathcal{H}_i)] + (1 - f_{\mathbf{w}}(\mathcal{H}^*))^+, \quad (1)$$

where \mathcal{H}^* is a heat map with all attributions as unity, and $\lambda > 0$ is a regularization hyperparameter. This DSF is obtained by training using the m attribution maps as input. Since \mathcal{H}^* is the heat map where any monotone function is maximized, the loss in the objective of Eqn (1) promotes functions/parameters that score all the baseline heat maps high. As a result, the scoring function, $f_{\mathbf{w}}$ will saturate already at heat maps that resemble the most specific heat maps among the given attribution maps that we ensemble. In order to prevent the trivial solution of $\mathbf{w} = \mathbf{0}$, we also put a constraint to control the scale of $f_{\mathbf{w}}$ such that $f_{\mathbf{w}}(\mathcal{H}^*) > 1$.

However, since in practice m is limited, we include further supervision in order to improve the generalization of (1). To this end, let's assume that the heat maps that we ensemble are binarized using k hard thresholds. We denote such binarized heat maps as $\mathcal{H}_i^j, i \in \{1, \dots, m\}, j \in \{1, \dots, k\}$. Let B_i^j denote the number of features selected in \mathcal{H}_i^j by the binary thresholding. We now propose our final formulation for learning the scoring function as:

$$\begin{aligned} \min_{\mathbf{w} \geq 0} \quad & \frac{\lambda}{2} \|\mathbf{w}\|^2 + \lambda_1 \left(\sum_{i=1}^m \left(f_{\mathbf{w}}(\mathcal{H}^*) - f_{\mathbf{w}}(\mathcal{H}_i) \right) \right) + \\ & \lambda_2 \left(\sum_{i=1}^m \sum_{j=1}^k \left(\delta + \max_{|A| \leq B_i^j} f_{\mathbf{w}}(A) - f_{\mathbf{w}}(\mathcal{H}_i^j) \right)^+ \right) \end{aligned} \quad (2)$$

where $\delta > 0$ is a hyperparameter controlling margin, and $(a)^+ \equiv \max(0, a)$. $\lambda > 0$, $\lambda_1 > 0$ & $\lambda_2 > 0$ are hyper-parameters. $\delta > 0$ helps in controlling the scale of $f_{\mathbf{w}}$ due to which we drop the scaling constraint used in equation (1). The new loss terms in Eqn (2) provide additional supervision to promote scores such that the binarized hard maps are scored high among the maps with the same number of selected feature. Note that the term $\max_{|A| \leq B_i^j} f_{\mathbf{w}}(A) - f_{\mathbf{w}}(\mathcal{H}_i^j)$ may turn out to be negative whenever the submodular maximization is solved approximately (e.g., when solved via the greedy algorithm). Hence the truncation based on the $(\cdot)^+$ is necessary in the proposed formulation (2).

As far as we know, formulations like Eqn (2) that jointly learn the submodular function as well as its concave extension are not well-studied in literature. We hope that the proposed formulation may be of independent interest in other applications where early saturating functions need to be induced for similar problems beyond attribution maps.

The proposed formulation (2) can be solved using Mirror Descent or Projected Subgradient Descent. Any subgradient of the objective in Eqn (2) is given by: $\lambda \mathbf{w} + \sum_{i=1}^m \left[\nabla_{\mathbf{w}} f_{\mathbf{w}}(\mathcal{H}^*) - \nabla_{\mathbf{w}} f_{\mathbf{w}}(\mathcal{H}_i) + \sum_{j=1}^k \rho_i^j \left(\nabla_{\mathbf{w}} f_{\mathbf{w}}(\bar{A}_i^j) - \nabla_{\mathbf{w}} f_{\mathbf{w}}(\mathcal{H}_i^j) \right) \right]$, where \bar{A}_i^j is a solution to the inner submodular maximization problem subject to cardinality constraint and $\rho_i^j > 0$ iff $\delta + \nabla_{\mathbf{w}} f_{\mathbf{w}}(\bar{A}_i^j) - \nabla_{\mathbf{w}} f_{\mathbf{w}}(\mathcal{H}_i^j) > 0$ and $\rho_i^j = 0$ otherwise. We solve for \bar{A}_i^j using the constant factor greedy approximation algorithm for maximization of a non-negative monotone submodular function [16]. Also, one can efficiently compute this subgradient by backpropagating through

the neural network modeling the DSF. We now discuss the algorithm for computing a new heat map that improves over the baselines using this induced scoring function.

3.2 Submodular Ensemble Attribution Algorithm

We begin by noting that high specificity in attribution heat maps cannot be achieved by arbitrary linear/non-linear combinations of the given heat maps. Also, considering scores of individual features may not help improve specificity in $f_{\mathbf{w}}$, as features may be redundant in the presence of others. Thus we propose to learn $f_{\mathbf{w}}$ that attributes features based on their marginal gain in the context of other features (i.e. $f_{\mathbf{w}}$ scores a subset of pixels rather than each individual pixel, which is a key difference from a linear combination of these heat maps). The proposed attribution algorithm is detailed in Algorithm (1). The algorithm is designed with the following key features/advantages: (i) It improves as the given heat maps that we ensemble improve; (ii) It is expected to achieve high specificity; (iii) By straightforward inheritance, the Axiom of ‘‘Implementation Invariance’’ defined in [28] is satisfied whenever the given heatmaps satisfy the same axiom; (iv) Since the proposed attributions are normalized, the axiom of completeness can be satisfied by appropriate scaling [28]; (v) Many types of other prior information can also be easily encoded as constraints in the proposed formulation (2). More specifically, one can insist that the proposed attribution satisfies the axioms Sensitivity(a) and/or Sensitivity(b) [28] by simply adding appropriate constraints in (2). For e.g., if the i^{th} feature needs to have non-zero attribution, one may include the constraint: $f_{\mathbf{w}}(\mathbf{1}) - f_{\mathbf{w}}(\mathbf{i}) \geq \epsilon$, where $\mathbf{1}$ is vector of all ones, and \mathbf{i} is vector of all ones except that the i^{th} entry is zero, and ϵ is a small tolerance. If this constraint is satisfied, the marginal gain of this feature w.r.t. any subset of features and hence the attribution value will be greater than or equal to ϵ , again because of the diminishing returns property. Analogously, if a feature, say v , must have zero attribution, then adding the constraint $f_{\mathbf{w}}(\{v\}) = f_{\mathbf{w}}(\mathbf{0})$ should suffice, where $\mathbf{0}$ is the vector of all zeros. (vi) Lastly, the proposed methodology offers some unique features like: (a) one can attribute a set of images (say, all examples of a particular class) by simply pooling all the attributions of all the images and learning the submodular score. This will be interesting because now features important at set (class) level will be revealed (b) If one needs to find p features that are most influential, then instead of picking the top- p attributed features, we can now solve for $\arg \max_{A \subseteq \{1, \dots, n\}, |A| \leq p} f_{\mathbf{w}}(A)$. This would give the top p discriminatory, yet non-redundant set of features.

Computational Effort The main computational overhead for the projected subgradient algorithm is the computation of $\bar{A}_i^j \forall i \in \{1, \dots, m\} \forall j \in \{1, \dots, k\}$. Interestingly, the use of the greedy algorithm ensures that computing \bar{A} for larger thresholds gives those for the smaller ones too. Hence at every iteration of the descent, only one call to the greedy algorithm needs to be made with cardinality bound as $B \equiv \max_{i \in \{1, \dots, m\}, j \in \{1, \dots, k\}} B_i^j$, leading to $O(Bn)$ evaluations of

Algorithm 1 Attribution Algorithm

Input: Trained DSF f , Set of features to be attributed V .
Initialize feature subset $A = \{\}$
Initialize $n = |V|$
Initialize attribution map $G[i] = 0$ for $i = 0, 1, \dots, n$
 $M = \{\arg \max_{v \in V \setminus A} f(v|A)\}$, Pick any $e \in M$
while $|A| < n$ and $f(e|A) > 0$ **do**
 for $p \in M$ **do**
 $G[p] = f(e|A)$
 end for
 $A = A \cup \{e\}$; $V = V \setminus M$
 $M = \{\arg \max_{v \in V} f(v|A)\}$, Pick $e \in M$
end while
for $p \in V$ **do**
 $G[p] = \frac{G[p]}{\sum_{p \in M} G[p]}$
end for

DSF output. Typically, $B \ll n$, leading to a marginal overhead of $O(n)$ DSF evaluations.

Scaling to High-dimensional Images We now discuss how DSF training can be scaled to high-resolution image data. The ideal choice would be to divide the image into regions of importance (segments), and reason at the level of segments than pixels, which would automatically also reduce the computational requirements. Segmentation algorithms, however, do not guarantee equal-sized segments. This restricts us from learning DSF as a function of segments. DSF is a monotonically non-decreasing function, so the greedy algorithm for cardinality-constrained maximization will be biased to pick a larger segment because of its larger marginal gain. We hence choose a careful sub-sampling approach as described below. As shown in Fig (2), our procedure for pre-processing high-dimensional inputs can be summarized in 4 stages: (1) obtaining attribution maps that we want to ensemble; (2) computing attribution scores for segments; (3) sub-sampling segmented attribution map & hard-thresholding the segments; (4) sub-sampling hard-thresholded segmented attribution map.

We now briefly describe each of these stages. In Step (2), we segment the given image and obtain segmented attribution maps with attribution score for a segment being the normalized sum of attribution scores of pixels present in that segment. A similar approach was earlier used in [10]. We then hard-threshold the segmented attribution map and obtain a set of segments in the top- k percentile and subsample this thresholded map to obtain (b), where each pixel can be considered equivalent to a window of pixels in the thresholded map of original resolution. In step (3), we subsample the segmented attribution map itself without hard-thresholding and obtain (a). We also tried sub-sampling thresholded attribution maps directly, but thresholding after segmentation gave better results.

The pre-processed inputs (a) and (b) are used in DSF training (Equation(2)) to provide heatmap level supervision and subset level supervision respectively.

After training the DSF, Algorithm (1) is used to compute our attribution map with V as the set of pixels in the sub-sampled resolution. We finally upsample this attribution map to match the original resolution of input image.

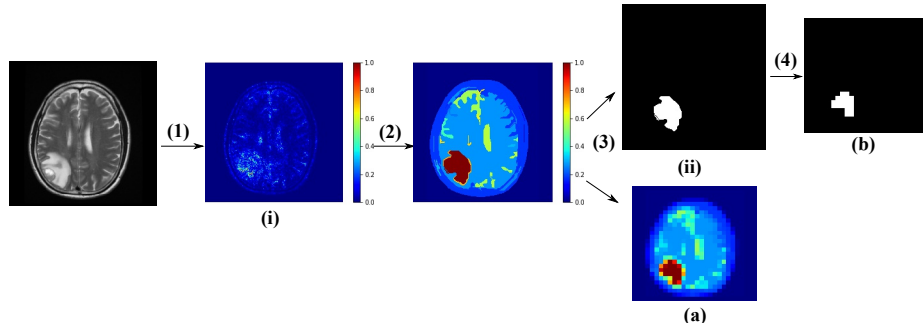


Fig. 2. Preprocessing for high-dimensional images: (a) & (b) are the pre-processed inputs for training DSF; (i) & (ii) are examples of \mathcal{H}_i & \mathcal{H}_i^j respectively in eq. (2).

Minimal Discriminative Region Size (MDRS) Metric We propose Minimal Discriminative Region Size (MDRS) metric & define it as the minimal number of pixels that are needed to perturb in order to change the class predicted by the classification network. An attribution algorithm with lower MDRS averaged across inputs can be expected to capture the discriminative regions with less number of false positives. MDRS with p as the perturbation value is defined as:

$$\text{MDRS}(p) = \min_{\mathbf{I}} |\mathbf{I}| \quad \text{s.t.} \quad y(\mathbf{x}) \neq y((1 - \mathbf{I}) \circ \mathbf{x} + (\mathbf{I} * p)) \quad (3)$$

where \mathbf{x} is the input image, $y(\mathbf{x})$ is the predicted class, and \mathbf{I} is a binary mask indicating which pixels to perturb. While not designed this way, MDRS can be seen as an extension of segment-level L_0 -attack [18], where we use attribution scores to compute the metric instead of using the gradient of neural network's loss. Its score can also be related to counterfactuals [29] when perturbed label is a specific label of interest. Like most other evaluation metrics for attribution, MDRS also assumes that the classifier is well-trained. In experiments, we obtain MDRS greedily by perturbing the segments in decreasing order of their importance.

Attrib Algorithm	BTD		CUB		Imagenet	
	Avg MDRS	Avg AUPC	Avg MDRS	Avg AUPC	Avg MDRS	Avg AUPC
Inp-Gr	25.56	29.19	NA	NA	NA	NA
IG	26.38	29.87	NA	NA	11.18	8.19
SIG	NA	NA	8.41	5.40	12.89	9.51
DL	26.08	29.72	8.03	5.29	10.57	7.51
GGC	27.52	30.91	8.30	5.40	15.32	11.14
GBP	NA	NA	9.54	6.30	NA	NA
DL-SHAP	26.08	29.72	NA	NA	10.56	7.52
Agg-Mean	26.14	29.68	8.36	5.45	11.32	8.30
CASO	25.46	29.31	8.00	5.22	15.18	11.29
SEA-NN	24.04	27.74	7.14	4.61	10.18	7.42

Table 1. Quantitative results for proposed SEA-NN method against 9 other attribution methods. Lower is better for MDRS and AUPC. Rank correlation $r_s = 0.90$ (pvalue=0.002) for BTD, $r_s = 0.94$ (pvalue=0.002) for CUB, and $r_s = 0.95$ (pvalue=0.0002) for ImageNet. Note that higher is better for rank correlation r_s .

4 Experiments

We used PyTorch for implementation and studied the proposed SEA-NN method against widely used methods such as IG [28], Inp-Gr [24], Smooth IG(SIG) [26], DeepLift (DL) [23], Guided Grad-CAM (GGC) [22], Guided Backprop GBP [27], DL-SHAP [13], Agg-Mean [20], and CASO [25]. We study these methods on three different datasets: ImageNet and Brain Tumor Detection and CUB. We also show some interesting qualitative results on MNIST.

Table (1) presents the quantitative results on all the three datasets. ‘NA’ denotes that a particular attribution method was not used as an input method for our SEA-NN algorithm on that dataset. We note that although SEA-NN and CASO require solving an optimization problem for every image, CASO needs a more careful hyperparameter tuning for every image separately to perform well but our algorithm performs well even when hyper-parameters were tuned on just 1-2 images. We also note that even though Smooth Grad variants are designed to be less noisy, we were able to outperform SIG in all our experiments. For all the experiments involving SIG, we compute it using 10 samples.

For all of these datasets, the time taken for pre-processing a high-dimensional input was 3.5 seconds, per-epoch training of DSF took 0.1 seconds & SEA-NN map generation took 0.8 seconds on an NVIDIA RTX 2080 Ti. Before pre-processing the input, we obtained the attribution maps that we wanted to ensemble using PyTorch’s Captum library [11]. For datasets other than MNIST, we pre-process the inputs according to the procedure described in section Scaling to High-dimensional Images. We chose the window size for sub-sampling as 8x8 and use 28x28 inputs to learn the DSF. For segmenting the images, we used Fenzenswalb’s algorithm [8]. In order to know how much each attribution map contributed towards the final scoring function, we pass the sub-sampled versions

of each of these attribution maps through our learnt DSF and rank them according to the scores given by the DSF. We mention this order of importance of attribution maps while describing our results for different datasets. The computation of both MDRS and AUPC was done by perturbing segments in the order of their relevance and setting all the pixels belonging to the perturbed segment as 0. We also compute the Spearman Rank Correlation (r_s) between MDRS and AUPC, as in Table (1)’s caption. In supplementary, we include detailed experimental setting, show more results. We comment on the choice of hyper-parameters in S4 and include ablation study on the initial DSF weights and the scale hyper-parameter used in segmentation.

4.1 Results on Imagenet

We used a pre-trained AlexNet model for Imagenet classification and experimented on the Imagenet validation data. As shown in Table(1), average MDRS as well as average AUPC is the lowest for our method compared to baseline methods. Qualitatively, we can see that we are able to highlight a sparser portion in the images that is the most relevant to the predicted class. Figure(1) shows that in the image belonging to the class ‘Mask’, our attribution map highlights all the masks present in the image but the other algorithms highlight a lot of unrelated regions too. The order of importance of attribution maps ensemble to learn the DSF was IG>DL>DL-Shap>Inp-Gr>GGC.

Human Interpretability on Imagenet We conducted an experiment to find if SEA-NN improves human interpretability. To evaluate the attribution maps on the basis of human interpretability, we use the human annotations provided by [14] for ninety eight images of the Imagenet dataset. We compute the Jaccard score between an attribution map and the annotated heat map after hard-thresholding them to keep only the top- k pixels. We compute this for multiple thresholds k and show the results in Table(2) which demonstrates that the relevant pixels picked by SEA-NN are the most human interpretable among all baselines.

Attribution Algorithm	15	50	100	200
IG	0.06	0.34	0.64	1.16
SIG	0.03	0.26	0.53	1.0
DL	0.04	0.20	0.38	0.72
GGC	0.07	0.29	0.57	1.07
DL-SHAP	0.04	0.20	0.38	0.72
SEA-NN	0.23	0.43	0.80	1.17

Table 2. Jaccard Score with human-annotated heatmaps (higher is better)

4.2 Results on Brain Tumor Detection dataset

We use a publicly available medical dataset, Brain Tumor Detection ¹ and use VGG-11 for our experiments. In the Brain Tumor Detection dataset, white mass inside the skull is known to be indicative of Brain Tumor. Figures (3) shows that SEA-NN correctly points out the infected regions. Sparsity is highly beneficial in medical diagnosis where false positives could be fatal. As shown in Table(1), the average MDRS score as well as the average AUPC score was the lowest compared to all the baselines. The order of importance of attribution maps ensemble to learn the DSF was INP-Gr>IG>DL>DL-Shap>GGC. Average MDRS and average AUPC of SIG were 25.75 & 29.91 respectively.

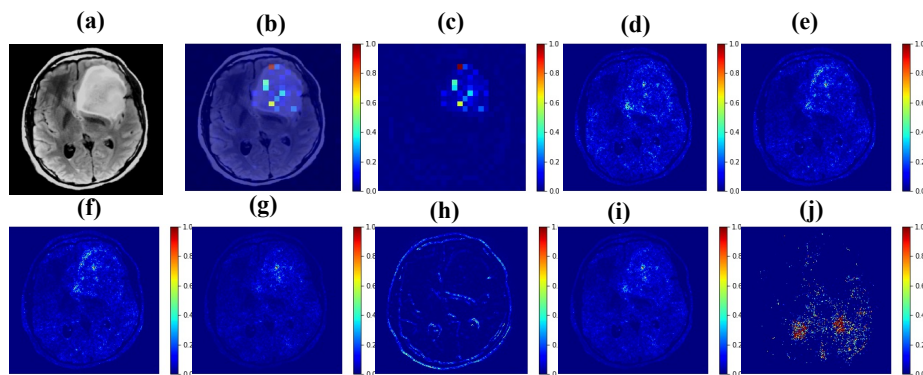


Fig. 3. (a) Image belonging to class Brain Tumor (b) SEA-NN overlaid on image (c) SEA-NN (d) Integrated gradients (e) Deep Lift (f) DeepSHAP (g) Input.Gradient (h) Guided Grad Cam (i) Agg-Mean (j) CASO

4.3 Results on CUB

We experimented on the standard test set of CUB dataset with Resnet-18. We achieved the best Avg MDRS and Avg AUPC among all the algorithms. Figure(9) shows that our attribution algorithm is sparser than the others and is able to capture the discriminative parts of the bird. The order of importance of attribution maps ensemble to learn the DSF was GGC>DL>GBP>SIG.

4.4 Discussions and Additional Experiments

These experiments were done on MNIST dataset. The experimental details are present in the Supplementary.

¹ <https://www.kaggle.com/navoneel/brain-mri-images-for-brain-tumor-detection>

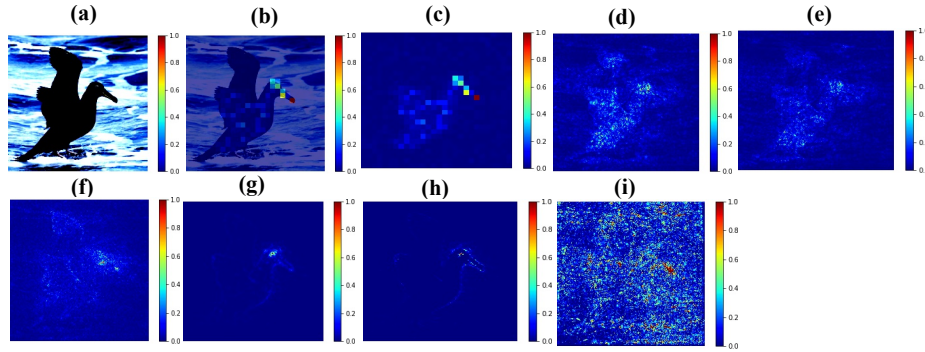


Fig. 4. (a) Image of a Sooty Albatross (b) SEA-NN overlaid on input (c) SEA-NN (d) SIG (e) DL (f) GBP (g) GGC (h) Agg-Mean (i) CASO

Visualizing The Top-k Pixels Figure(5) shows the difference between the top-10 pixels selected by the attribution maps that we ensemble and the top-10 pixels selected by cardinality constrained maximization of our learnt DSF. We note that the latter set of pixels is the same as the top-k pixel’s of SEA-NN. Besides highlighting more discriminative & less redundant pixels, the example of digits 6 & 2, shows the efficacy of ensembling attribution maps.

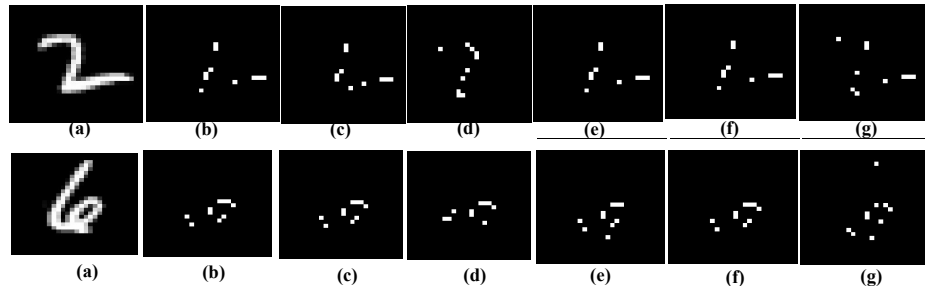


Fig. 5. (a) Input; Top-10 pixels of attribution maps to ensemble (b) Inp Gr (c) IG (d) GGC (e) DL Shap (f) DL (g) top-10 pixels of SEA-NN ie. $\operatorname{argmax}_{A \subseteq V, |A| \leq 10} (f_w(A))$

Global Attribution map We performed qualitative experiments to see the performance of SEA-NN as a global attribution algorithm. Most of the existing attribution algorithms are local in nature (i.e. pertain to a particular input). Local attribution algorithm tries to explain a specific input, while global attribution algorithm provides a more holistic view by giving an explanation for all images of the same class present in the dataset.

To get a global attribution map, we simply expand our training set to include attribution maps of all images of a given class and hence learn a global scoring function. Using this learned scoring function and using algorithm(1), we generate a global attribution map. We present the results in S5 of Supplementary owing to space constraints.

5 Conclusion

We propose a framework to improve the existing attribution methods and introduce a novel model-agnostic Submodular attribution method, SEA-NN, capable of providing both local and global explanations. Better specificity makes SEA-NN one of the best choices for critical domains where penalty on false positives is high. Ensembling attribution maps of different methods is a promising way to reduce epistemic uncertainty and biases associated with each attribution method. The special properties satisfied by our learnt scoring function and the ease of adding additional constraints during training makes it suitable for needs of different users. Moreover, we also present a simple yet novel metric, MDRS, that simultaneously quantifies the discriminative power and the specificity of an attribution method.

In our future work, we would explore a transfer learning approach where DSF trained on a few inputs can be finetuned on new ones.

S1 Attribution Algorithms For Ensembling

We describe the different attribution methods that we use to ensemble and obtain SEA-NN. We represent the input as $x \in \mathbb{R}^d$, the classification network as $f : \mathbb{R}^d \rightarrow \mathbb{R}^C$ where C is the number of classes. y is used to denote the classification network’s output for the class whose attribution map we are interested in.

Inp-Gr: Gradient◦Input(Inp-Gr) renders $x \circ \frac{\partial y}{\partial x}$ as the attribution map.

IG: Integrated Gradients or IG along i^{th} dimension for input x and baseline x' is given by:

$$\text{IG}_i(x) := (x_i - x'_i) \int_{\alpha=0}^1 \frac{\partial y(x' + \alpha(x - x'))}{\partial x_i} \partial \alpha$$

SIG: Smooth Grad version of IG (**SIG**), produces less noisy attribution maps by taking an average of attribution scores assigned to $x + n_j$ such that $n_j \sim \mathcal{N}(0, \sigma^2)$ for $j = 1 \dots N$. We take N as 10 in our experiments.

DL: We use DeepLift’s rescale rule in our experiments which we describe below:

- $z_{ji} = w_{ji}^{(l+1,l)} x_i^l$: weighted activation of a neuron i onto neuron j in the next layer.
- $\bar{z}_{ji} = w_{ji}^{(l+1,l)} \bar{x}_i^l$: weighted activation of a neuron i onto neuron j in the next layer, when baseline \bar{x} fed as the input.
- $r_i^{(l)}$: relevance of unit i on layer l

- L : the output layer

The attribution scores are finally computed as:

$$r_i^{(L)} = y_i(x) - y_i(\bar{x}) \text{ if unit } i \text{ is target unit of interest} = 0 \text{ otherwise.}$$

$$r_i^{(l)} = \sum_j \frac{z_{ji} - \bar{z}_{ji}}{\sum_{i'} (z_{ji'} - \bar{z}_{ji'})} r_j^{(l+1)}$$

DeepShap or DeepLift Shap (**DL-Shap**) takes distribution of baselines and averages DeepLift attributions per input example resulting from each input-baseline pair.

GBP: For a given input, Guided Backprop GBP backpropagates the gradients of y with respect to x till the input layer, zeroing out gradients which are negative or which correspond to negative activations.

GGC: Guided GradCAM (GGC) attribution scores are element-wise product of GBP attribution scores and GradCAM attribution scores. GradCAM mask is given by $\text{ReLU}(\sum_k \alpha^k A^k)$ where A^k 's are the feature maps obtained from the last convolutional layer of f and $\alpha^k = \frac{1}{Z} \sum_i \sum_j \frac{\partial y}{\partial A_{i,j}^k}$.

S2 Deep Submodular Function

A Deep Neural Network(DNN) whose weights are restricted to be non-negative and the activation functions used are monotone non-decreasing concave for non-negative reals, constitutes a non-negative monotone non-decreasing submodular function when given Boolean input vectors. This is referred to as Deep Submodular Function (DSF) that can be trained in the similar way as DNNs. The key result that forms the basis of DSF is that sums of concave functions, composed with modular functions (SCMMs), can be easily shown to be submodular. For more details, we urge interested readers to refer to Section 3 in [6].

S3 Detailed Experimental Setting

We chose DSF as a 4-layer Feed-forward neural network for experiments across all the datasets. The DSF architecture used for all experiments was Linear(784, 512) \rightarrow sqrt \rightarrow Linear(512, 128) \rightarrow sqrt \rightarrow Linear(128, 32) \rightarrow sqrt \rightarrow Linear(32, 1), where sqrt denotes square root function used as the activation function. For Brain Tumor Detection experiment, we added an additional square root activation to the output of the last layer. Adam was used as the optimizer for training the DSF in all our experiments with weight decay as 10^{-6} . DSF's initial weights were sampled from a uniform distribution between 2 and 2.25.

Imagenet The value of λ , λ_1 , λ_2 were 10^{-5} , 10, 0.01 and DSF was trained for 20 epochs. The value of δ was 10^{-7} the set of percentiles used for thresholding was {97,97.5,98,98.5,99,99.5}. Scale hyper-parameter for segmentation was 500. For CASO, λ_1 was chosen to be 0.02 and the smoothness argument was set.

Brain Tumor Detection We fine-tuned a pre-trained VGG-11 network. The validation accuracy at the end of training was 82%. Value of δ was 10^{-5} , λ was chosen as 1, λ_1 as 10 and λ_2 as 0.1, δ was 10^{-5} . The DSF was trained

for 20 epochs. For CASO, λ_1 was chosen to be 0.002 and the smoothness argument was set. The set of percentiles used for thresholding attribution maps was $\{97, 97.5, 98, 98.5, 99, 99.5\}$. Scale hyper-parameter for segmentation was 500.

CUB We fine-tuned Resnet-18 to obtain 72% top-1 accuracy and 93% top-5 accuracy. δ was 10^{-6} and $\lambda, \lambda_1, \lambda_2$ were 1, 10, 0.1 respectively. The set of percentiles used for hard-thresholding the attribution maps was $\{97, 97.5, 98, 98.5, 99, 99.5, 99.6, 99.7\}$ and the DSF was trained for 50 epochs. Scale hyper-parameter for segmentation was 1000. For CASO, λ_1 was chosen to be 10^{-4} and the smoothness argument was set.

S4 Observations with Choice of Hyperparameters

Following are the main observations that we came across related to the choice of hyperparameters involved in Deep Submodular Function (DSF) training:

- **Choice of DSF architecture:** We observed that using a feedforward architecture gave much better results than using convolutional architecture for DSF. As shown in section 4 of the main paper, with a simple 4-layer feedforward DSF, we were able to outperform all baseline attribution methods.
- **Choice of activation functions:** To learn a DSF, we need a concave monotone non-decreasing non-negative activation function. In our experiments, we tried using $g(x) = \sqrt{x}$ and $g(x) = \log(1 + x)$ as the activation functions. Having $g(x) = \log(1 + x)$ in the middle layers of DSF architecture provided smoother attribution maps, but the results with $g(x) = \sqrt{x}$ activation function were quantitatively better and qualitatively comparable to $g(x) = \log(1 + x)$.
- **Training epochs:** As we mention in section 3.2 of the main paper, the ease of incorporating prior knowledge while training the DSF makes our approach flexible enough to cater to the needs of a variety of users. Let’s say the user wants to ensemble maps of attribution methods A_i ’s such that the obtained SEA-NN map highlights the boundaries of the objects belonging to the class of interest. If literature supports a specific attribution method j (say) as the ideal choice for this purpose, then the user can choose to train the DSF until the score given by DSF to A_j is the highest. In the absence of such prior knowledge, the number of epochs of DSF training can be decided based on the objective-over-epoch curve.
- **Initial weights:** Learning a DSF requires the weights to be non-negative. Hence, we choose to sample the initial weights from a uniform distribution between hyperparameters $a > 0$ and $b > 0$. Following the convention of initializing the weights close to 0, we avoid choosing large values for b and a .
- **Selection of attribution methods:** We chose these based on widely used methods in literature today, as well as initial empirical studies of qualitative assessment of attribution maps obtained by these methods.
- **Scaling up:** Our approach for scaling to high-dimensional images needs segmenting the image for which we use the Felzenszwalb’s algorithm specifying

the ‘Scale’ hyperparameter. We observed that among all the hyperparameters, scale was the most influential towards the quantitative results. This is expected since our algorithm assigns context-aware attribution scores and scale controls the size of the segments which determines the amount of context captured by that segment.

S5 More Results on MNIST

We present more results of global attribution maps in Figure 7. These attribution maps are obtained by ensembling the attribution maps (based on the score provided by our trained DSF model) of all images belonging to a given class, across all methods. We believe that training the DSF based on k -nearest neighbors belonging to a given class will result in smoother global attribution maps. Following the popular practice of multiplying input with the heat map, we present results in Figure 8. We also show the top influential pixels on a few individual images in Figure 6, which are obtained by querying the top- k most important pixels by our method and the other attribution methods which we ensemble. We can see that for the same budget (cardinality constraint), SEA-NN picks a more diverse set of pixels which can be used to classify the input image. The top- k pixels chosen by SEA-NN is given by $\operatorname{argmax}_{A \in V, |A| \leq k} (f_{\mathbf{w}}(A))$.

The usefulness of our method is evident for complex datasets, as shown in all our results so far. Note that the MNIST dataset is however a good testbed to present global attribution maps since all objects (digits in this case) are present in almost the same location in the image. For the experiments on MNIST, we trained a 4-layer feedforward network with convolutions to classify MNIST with a test error of $\sim 2\%$. The initial weights for DSF were sampled from $\mathcal{U}(2, 2.25)$. For training the DSF, we take attribution maps of IG, DL, DL-Shap, Input.gradient and GGC. We used $g(x) = \log(1 + x)$ as the activation function after the first three layers, the last layer had $g(x) = x$ as the activation function. δ was 10^{-6} and the DSF was trained for 20 epochs.

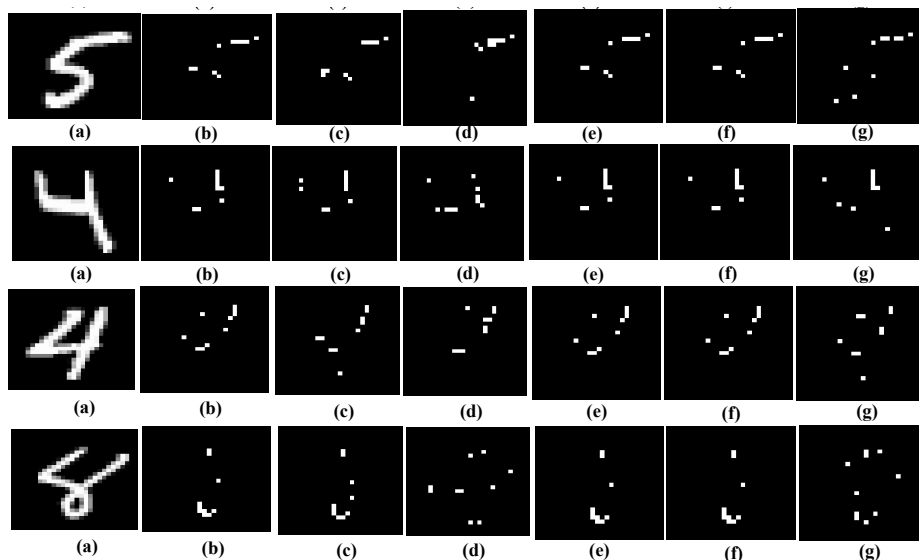


Fig. 6. (a) Input; Top-10 pixels of: (b) Inp Gr (c) IG (d) GGC (e) DL Shap (f) DL (g) top-10 pixels of SEA-NN ie. $\text{argmax}_{A \subseteq V, |A| \leq 10} (f_w(A))$

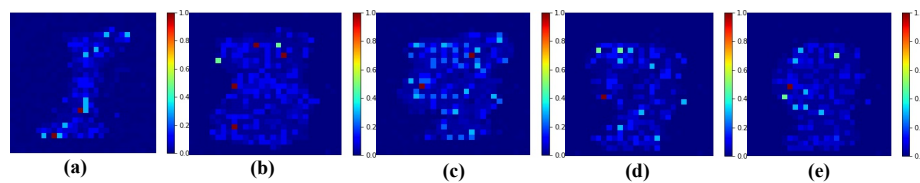


Fig. 7. More results on MNIST: Global attribution map for (a) class 1 (b) class 3 (c) class 4 (d) class 7 (e) class 9

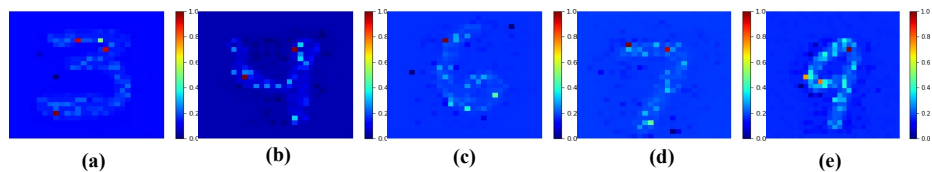


Fig. 8. Global attribution maps multiplied by corresponding inputs for (a) class 3 (b) class 4 (c) class 6 (d) class 7 (e) class 9

S6 More Results on CUB

In continuation to the results included in section 4.3 of the main paper, we present more qualitative results and some ablation studies on CUB. Figure 9 shows attribution maps for 3 images taken from the CUB test set: (1) belonging to the class ‘Clay colored sparrow’; (2) belonging to the class ‘Pine Grosbeak’; and (3) belonging to the class ‘Parakeet Auklet’. The maps of SEA-NN highlight the non-redundant pixels corresponding to the discriminative parts of the birds, even in the presence of more than one instance of the object of interest.

We also present ablation studies on the initial weights for DSF training, scale of segmentation and choice of attribution maps.

Ablation on initial weights: We show that SEA-NN outperforms the baseline attribution methods even with different choices of initial weights for DSF. In Table 1 of the main paper, we showed the results with initial weights sampled from $\mathcal{U}(2, 2.25)$. In Table 3, we denote SEA-NN(a, b) to show results of SEA-NN with initial weights sampled from $\mathcal{U}(a, b)$. Weights are chosen to be close to 0 following the standard conventions. As shown in the table, SEA-NN performs the best among all baselines even with the choices of different initial weights.

Ablation on scale of segmentation: In Table 1 of the main paper, we showed results with scale hyperparameter for segmentation as 1000. We repeated the experiments with scales 50, 150 and 2000 and the results are shown in Table 4. We get the best Avg MDRS & Avg AUPC scores with scale chosen as 150 and 2000 also. Unlike the Brain Tumor Detection dataset where the object of interest (tumor) is usually small in size, we can expect the segments obtained with scale as 50 to be too small to capture semantically meaningful context in the CUB dataset. Hence, context-aware attribution maps of SEA-NN don’t provide much improvement over the baselines when scale is chosen to be 50 in CUB. As shown in the caption for Table 4, the rank correlation between MDRS and AUPC remains high.

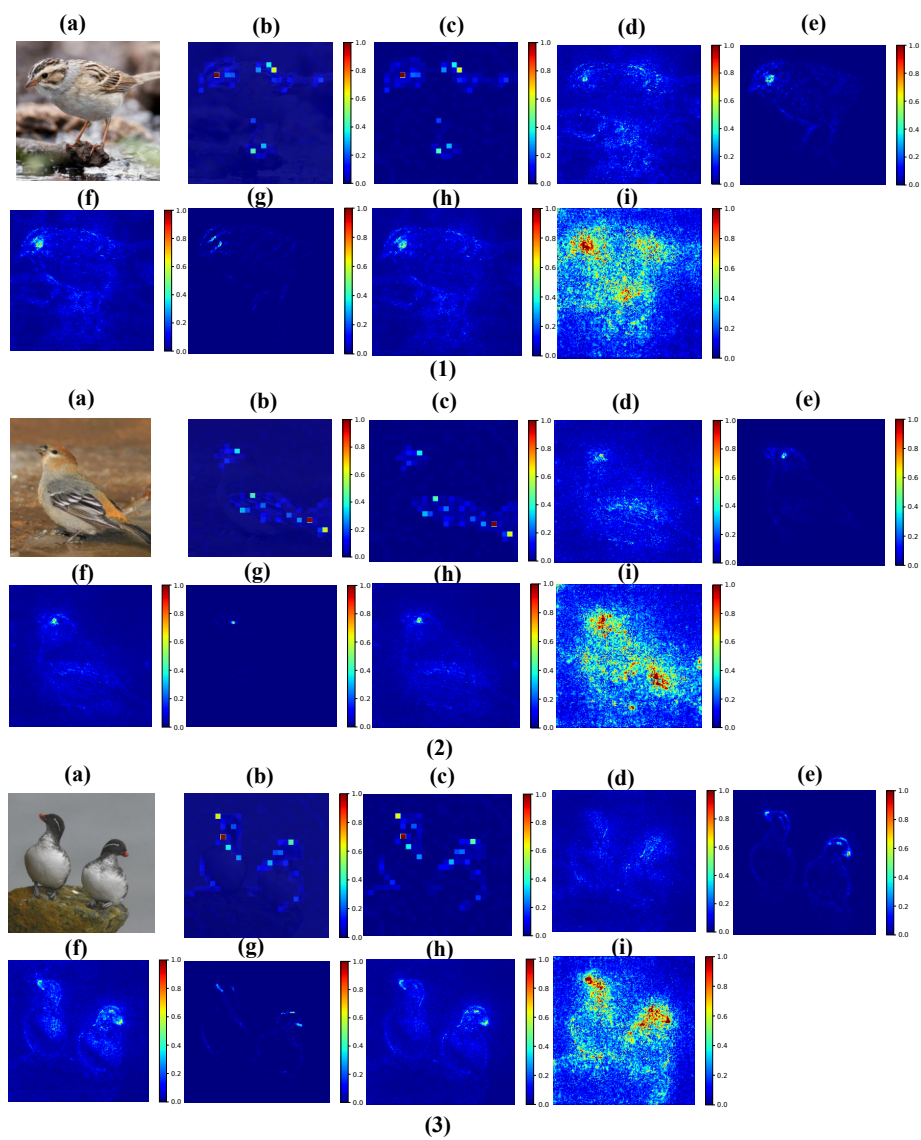


Fig. 9. More results on CUB: (a) Image from CUB (b) SEA-NN overlaid on input (c) SEA-NN (d) SIG (e) DL (f) GBP (g) GGC (h) Agg-Mean (i) CASO

Attribution Algorithm	Avg MDRS	Avg AUPC
SIG	5.40	12.89
DL	8.03	5.29
GGC	8.30	5.40
GBP	9.54	6.30
Agg-Mean	8.36	5.45
CASO	8.00	5.22
SEA-NN	7.14	4.61
SEA-NN(2, 4)	7.15	4.63
SEA-NN(4, 4.25)	7.16	4.62
SEA-NN(0.75, 1)	7.17	4.64

Table 3. Ablation on DSF’s initial weights for CUB. Lower is better for MDRS and AUPC.

Attrib Algorithm	scale 50		scale 150		scale 2000	
	Avg MDRS	Avg AUPC	Avg MDRS	Avg AUPC	Avg MDRS	Avg AUPC
SIG	36.99	28.43	19.20	13.94	7.22	4.59
DL	34.25	27.02	18.79	14.06	6.7	4.32
GGC	44.73	34.72	24.76	18.22	7.81	5.06
GBP	32.04	25.39	18.29	13.52	7.11	4.59
Agg-Mean	30.38	24.21	17.40	12.88	7.22	4.66
CASO	33.1	26.00	17.09	12.69	6.94	4.47
SEA-NN	32.50	25.97	16.91	12.61	6.45	4.10

Table 4. Ablation results on CUB for different scales for segmentation. Lower is better for MDRS and AUPC. Rank correlation $r_s = 1$, $r_s = 1$, $r_s = 0.94$ for scales 50, 200 and 1000 respectively. Note that higher is better for rank correlation r_s .

S7 More Results on Imagenet

In Figure 10, we qualitatively compare the attribution maps for 3 images: (1) belonging to the class ‘Grand Piano’; (2) belonging to the class ‘Flute’; and (3) belonging to the class ‘Cucumber’. Unlike other methods which also highlight some portion of the person’s hand holding the Cucumber, SEA-NN maps more specifically highlight only the Cucumber in the image belonging to the class ‘Cucumber’. Besides being more specific in all the 3 images, we note that SEA-NN maps accurately highlight multiple flutes present in the image belonging to the class ‘Flute’. For the images of Piano and Flute, the CASO resulted in blank maps, hence we did not include them here. As noted earlier in section 4 of the main paper, the hyperparameters of CASO needs more careful tuning for solving an optimization for each image, which is a key limitation.

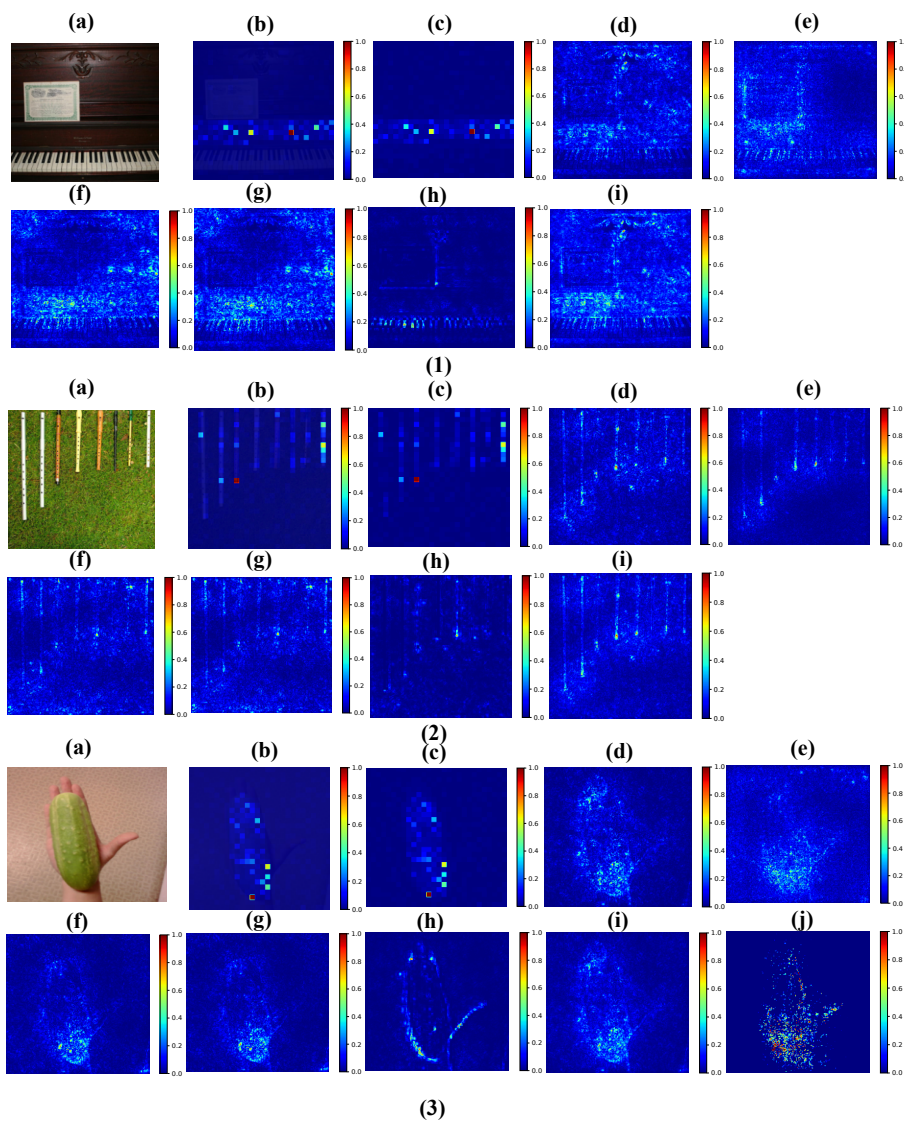


Fig. 10. More results on ImageNet: (a) Image from Imagenet (b) SEA-NN overlaid on image (c) SEA-NN (d) IG (e) SIG (f) DL (g) DL-SHAP (h) GGC (i) Agg-Mean

S8 More Results on BTD

Figure 11 shows more examples of high specificity and high discriminative power of SEA-NN maps as they highlight the infected regions of Tumor with less false

positives. Table 6 presents ablation with scale of segmentation where we can see that SEA-NN outperforms the baseline methods even with smaller and larger scales. We now present the ablation study on the choice of initial weights of DSF. We reported results in Table 1 of the main paper with initial weights sampled from $\mathcal{U}(2, 2.25)$. In Table 5, we show quantitative results with SEA-NN(a, b) which corresponds to initial weights being sampled from $\mathcal{U}(a, b)$ keeping the rest of the hyperparameters the same. SEA-NN outperforms baseline methods, irrespective of the choice of initial weights.

Attribution Algorithm	Avg MDRS	Avg AUPC
Inp-Gr	25.56	29.19
IG	26.38	29.87
SIG	25.75	29.91
DL	26.08	29.72
GGC	27.52	30.91
DL-SHAP	26.08	29.72
AVG	26.14	29.68
CASO	25.46	29.31
SEA-NN	24.04	27.74
SEA-NN(2, 4)	22.089	26.495
SEA-NN(4, 4.25)	25.162	28.273
SEA-NN(0.75, 1)	23.508	27.828
SEA-NN(1, 10)	20.953	24.690

Table 5. Ablation on DSF’s initial weights for BTD. Lower is better for MDRS and AUPC.

Attrib Algorithm	scale 50		scale 200		scale 1000	
	Avg MDRS	Avg AUC	Avg MDRS	Avg AUC	Avg MDRS	Avg AUC
Inp-Gr	115.51	174.45	190.17	273.28	154.9	228.83
IG	115.6	174.43	194.39	275.01	155.94	229.33
DL	113.33	168.94	190.65	268.49	153.7	223.13
GGC	127.82	177.53	216.02	281.66	173.07	225.0
DL-SHAP	113.33	168.94	190.65	268.49	153.7	223.13
Agg-Mean	123.44	174.48	205.69	277.2	169.21	231.50
CASO	117.53	170.26	195.03	267.62	159.62	225.0
SEA-NN	108.95	161.06	179.57	252.37	147.17	212.62

Table 6. Ablation results on BTD for different scales for segmentation. Lower is better for MDRS and AUC. Rank correlation $r_s = 0.9$, $r_s = 0.69$, $r_s = 0.93$ for scales 50, 200 and 1000 respectively. Note that higher is better for rank correlation r_s .

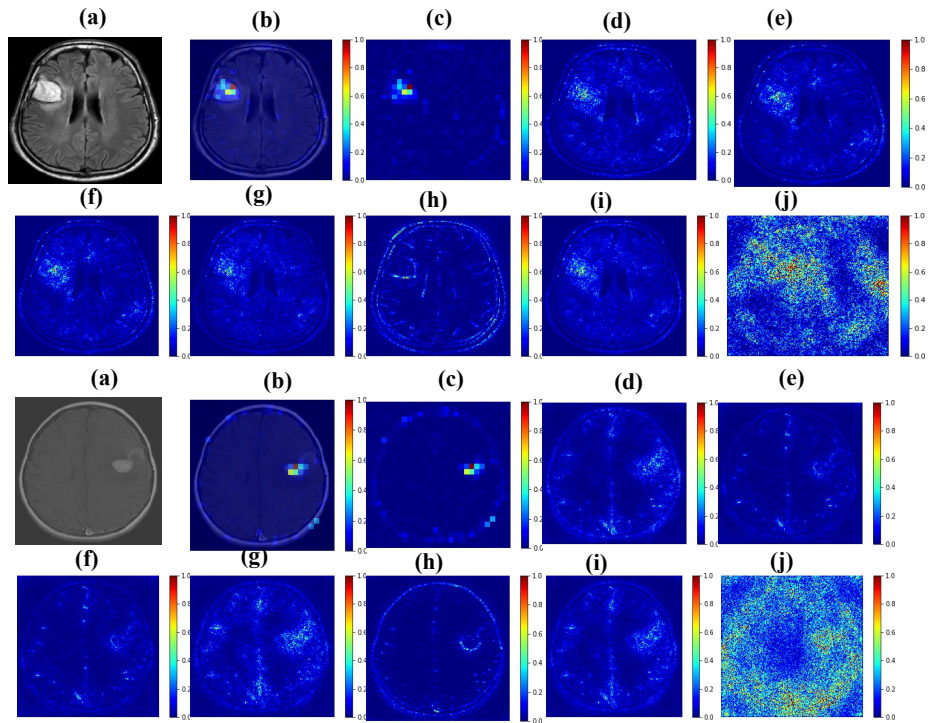


Fig. 11. More results on BTB: (a) Image belonging to class Brain Tumor (b) SEA-NN (Proposed attribution map) overlaid on image (c) SEA-NN (d) Integrated gradients (e) Deep Lift (f) DeepSHAP (g) Input.Gradient (h) Guided Grad Cam (i) Agg-Mean (j) CASO

S9 More SEA-NN attribution maps on CUB & Imagenet

In Figure 12, we present some more SEA-NN attribution maps overlaid on images for CUB & Imagenet datasets. The first row corresponds to the images from CUB & the second row corresponds to the images from Imagenet dataset. The class names are mentioned in the caption.

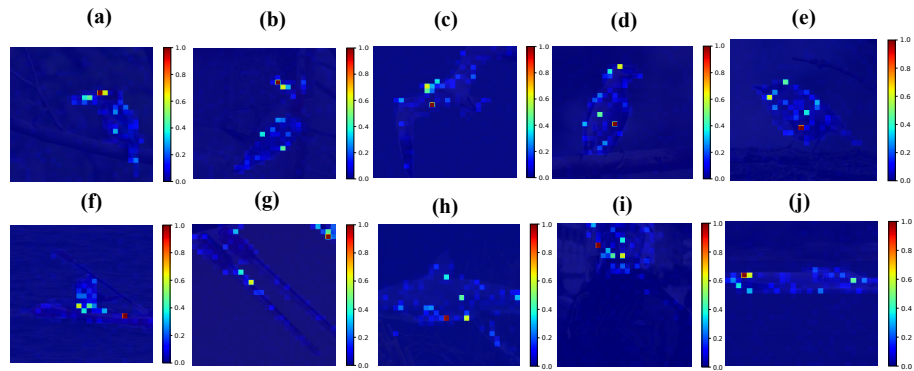


Fig. 12. (a)White Breasted Kingfisher (b)Red Bellied Woodpecker (c)Caspian Tern (d)Cedar Waxwing (e)House Wren (f)Paddle (g)Screwdriver (h)Great White Shark (i)Gas-mask (j)Speedboat

References

1. Alvarez-Melis, D., Jaakkola, T.S.: Towards robust interpretability with self-explaining neural networks. CoRR [abs/1806.07538](https://arxiv.org/abs/1806.07538) (2018), <http://arxiv.org/abs/1806.07538>
2. Bhatt, U., Weller, A., Moura, J.M.F.: Evaluating and aggregating feature-based model explanations (2020)
3. Chattopadhyay, A., Manupriya, P., Sarkar, A., Balasubramanian, V.N.: Neural network attributions: A causal perspective. In: Proceedings of the 36th International Conference on Machine Learning (2019)
4. Chattopadhyay, A., Sarkar, A., Howlader, P., Balasubramanian, V.N.: Grad-cam++: Generalized gradient-based visual explanations for deep convolutional networks. CoRR [abs/1710.11063](https://arxiv.org/abs/1710.11063) (2017)
5. Chen, C., Li, O., Tao, D., Barnett, A., Rudin, C., Su, J.K.: This looks like that: Deep learning for interpretable image recognition. In: Advances in Neural Information Processing Systems 32 (2019)
6. Dolhansky, B.W., Bilmes, J.A.: Deep submodular functions: Definitions and learning. In: Advances in Neural Information Processing Systems 29 (2016)
7. Elenberg, E., Dimakis, A.G., Feldman, M., Karbasi, A.: Streaming weak submodularity: Interpreting neural networks on the fly. In: Advances in Neural Information Processing Systems 30 (2017)
8. Felzenszwalb, P.F., Huttenlocher, D.P.: Efficient graph-based image segmentation. International Journal of Computer Vision (2004)
9. Hooker, S., Erhan, D., Kindermans, P., Kim, B.: A benchmark for interpretability methods in deep neural networks (2019), <http://papers.nips.cc/paper/9167-a-benchmark-for-interpretability-methods-in-deep-neural-networks>
10. Kapishnikov, A., Bolukbasi, T., Viegas, F., Terry, M.: Xrai: Better attributions through regions. In: The IEEE International Conference on Computer Vision (ICCV) (2019)

11. Kokhlikyan, N., Miglani, V., Martin, M., Wang, E., Reynolds, J., Melnikov, A., Lunova, N., Reblitz-Richardson, O.: Pytorch captum. <https://github.com/pytorch/captum> (2019)
12. Krause, A., Golovin, D.: Submodular function maximization. (2014)
13. Lundberg, S.M., Lee, S.I.: A unified approach to interpreting model predictions. Curran Associates, Inc. (2017), <http://papers.nips.cc/paper/7062-a-unified-approach-to-interpreting-model-predictions.pdf>
14. Mohseni, S., Ragan, E.D.: A human-grounded evaluation benchmark for local explanations of machine learning. CoRR **abs/1801.05075** (2018)
15. Montavon, G., Bach, S., Binder, A., Samek, W., Müller, K.: Explaining nonlinear classification decisions with deep taylor decomposition. CoRR **abs/1512.02479** (2015)
16. Nemhauser, G.L., Wolsey, L.A., Fisher, M.L.: An analysis of approximations for maximizing submodular set functions - I. Math. Program. **14**(1) (1978)
17. Petsiuk, V., Das, A., Saenko, K.: Rise: Randomized input sampling for explanation of black-box models. In: Proceedings of the British Machine Vision Conference (BMVC) (2018)
18. Ren, K., Zheng, T., Qin, Z., Liu, X.: Adversarial attacks and defenses in deep learning. Engineering **6**(3), 346–360 (2020). <https://doi.org/https://doi.org/10.1016/j.eng.2019.12.012>, <https://www.sciencedirect.com/science/article/pii/S209580991930503X>
19. Ribeiro, M.T., Singh, S., Guestrin, C.: Why should i trust you?: Explaining the predictions of any classifier. In: Proceedings of the 22nd ACM SIGKDD International Conference on Knowledge Discovery and Data Mining. pp. 1135–1144. ACM (2016)
20. Rieger, L., Hansen, L.K.: Aggregating explainability methods for neural networks stabilizes explanations. CoRR **abs/1903.00519** (2019), <http://arxiv.org/abs/1903.00519>
21. Rieger, L., Hansen, L.K.: A simple defense against adversarial attacks on heatmap explanations (2020)
22. Selvaraju, R.R., Das, A., Vedantam, R., Cogswell, M., Parikh, D., Batra, D.: Grad-cam: Why did you say that? arXiv preprint arXiv:1611.07450 (2016)
23. Shrikumar, A., Greenside, P., Kundaje, A.: Learning important features through propagating activation differences. arXiv preprint arXiv:1704.02685 (2017)
24. Simonyan, K., Vedaldi, A., Zisserman, A.: Deep inside convolutional networks: Visualising image classification models and saliency maps. In: 2nd International Conference on Learning Representations, ICLR Workshop (2014)
25. Singla, S., Wallace, E., Feng, S., Feizi, S.: Understanding impacts of high-order loss approximations and features in deep learning interpretation. In: Proceedings of the 36th International Conference on Machine Learning, ICML (2019)
26. Smilkov, D., Thorat, N., Kim, B., Viégas, F., Wattenberg, M.: SmoothGrad: removing noise by adding noise. ICML workshop on visualization for deep learning (Jun 2017)
27. Springenberg, J.T., Dosovitskiy, A., Brox, T., Riedmiller, M.A.: Striving for simplicity: The all convolutional net. In: 3rd International Conference on Learning Representations, ICLR Workshop (2015)
28. Sundararajan, M., Taly, A., Yan, Q.: Axiomatic attribution for deep networks. In: Proceedings of the 34th International Conference on Machine Learning (2017)
29. Verma, S., Dickerson, J., Hines, K.: Counterfactual explanations for machine learning: A review (2020)

30. Zeiler, M.D., Fergus, R.: Visualizing and understanding convolutional networks. CoRR **abs/1311.2901** (2013), <http://arxiv.org/abs/1311.2901>
31. Zhang, Q., Nian Wu, Y., Zhu, S.C.: Interpretable convolutional neural networks. In: The IEEE Conference on Computer Vision and Pattern Recognition (CVPR) (June 2018)
32. Zhou, B., Khosla, A., Lapedriza, À., Oliva, A., Torralba, A.: Learning deep features for discriminative localization. In: IEEE Conference on Computer Vision and Pattern Recognition, CVPR (2016)